Data-Driven Dynamic Modeling for a Swimming Robotic Fish

Junzhi Yu, *Senior Member, IEEE*, Jun Yuan, Zhengxing Wu, and Min Tan

***Abstract*—This paper proposes a data-driven dynamic modeling method for multijoint robotic fish with irregular geometric profiles and numerous heterogeneous hydrodynamic parameters. The method is composed of two main components: dynamic modeling and hydrodynamic parameter identification. In dynamic modeling, fluid forces exerted on the robotic fish are analyzed by the Morrison equation and the strip method. A dynamic model with an explicit formulation is derived, in which all terms involved in the dynamic analysis are converted to the coordinate system attached to the head. Further, the parameter identification technique is integrated into dynamic modeling, which reshapes it with data-driven feature and thereby makes it be competent to model swimming robots with complex geometric profiles and numerous heterogeneous hydrodynamic parameters. Experimental data of the swimming robotic fish are collected to identify the parameters directly. The obtained dynamic model is validated by data captured under extensive motion modes like forward swimming, varying velocity, and turning. Comparisons of simulated and experimental results demonstrate the effectiveness of the method.**

***Index Terms*—Hydrodynamic analysis, modeling and control, parameter identification, robotic fish.**

I. Introduction

THROUGH long-term evolution and natural selection, fish possess remarkable ability to interact with the aquatic environments. Their attractive features have aroused great interest in the research on bio-inspired robotic fish in the last decades, including propulsive mechanisms, control algorithms [1]–[3], underwater localization [4], [5], etc. In particular, dynamic modeling [6]–[12] is a valuable research topic, since dynamic models can offer guidance for almost all other research or applications related to robotic fish.

It is through interacting with surrounding fluid that robotic fish achieve various locomotion. The most complicated and challenging problem of dynamic modeling lies in capturing the hydrodynamics [8], [9], [13]. Existing methods for hydrodynamic modeling can be divided to two classes: numerical methods and analytical methods. Numerical methods require solving the Navier–Stokes equations, which are accurate but extremely time-consuming. By contrast, analytical modeling methods are more feasible and practical for robotics. The first analytical model of fish swimming is the resistive theory [14]. In this model, the fluid forces are composed of longitudinal skin friction and lateral drag forces. But the resistive theory does not take inertia forces into consideration. The waving plate theory [15] analyzes the hydrodynamics by modeling fish as an undulating infinite height plate. In comparison with the waving plate theory, Lighthill's theory [16]–[18] is more pertinent for modeling of swimming robots, including the elongated body theory (EBT) and the large amplitude elongated body theory (LAEBT). The EBT captures the added mass effect and approximates the effect of wake dynamics based on the kinetic momenta balance in a hemisphere control volume containing the fish body. The LAEBT extends the EBT to the cases of large amplitude body deformations. Owing to its simplicity and effectiveness, Lighthill's theory has been widely utilized in hydrodynamic modeling of robotic fish [8], [12], [19]. Additionally, the quasi-steady lift and drag models from airfoil theory are also commonly used hydrodynamic modeling methods for bodies or fin surfaces of robotic fish [10], [20].

Hydrodynamic parameters are crucial for an accurate dynamic model of robotic fish. Undoubtedly, how to obtain the hydrodynamic parameters is an inevitable problem in hydrodynamic modeling. In general, four types of approaches have been utilized in previous literature: estimating by existing standard cases [6], [8], calculating by computational fluid dynamics (CFD) simulations [20], performing experimental measurements [11], [19], [21], and identifying from motion data [10]. In the first method, the parameters are estimated through approximating a robotic fish by standard shapes whose hydrodynamic parameters are already available under certain fluid conditions. But it is not appropriate to robots with irregular and complex geometric profiles, since no references can help to determinate the parameters. The CFD method requires the shape model of a robotic fish and outputs a theoretical result, which is not necessarily in accord with the actual situation. Regarding the method of experimental measurements, particular measuring instruments are required, and the measurements are basically restricted to drag and thrust coefficients. In contrast, it may be practical and convenience to identify parameters directly from motion data, which can be captured simply by video cameras or on-board sensors with the robotic fish swimming freely. Indeed, identification approaches have been widely studied for

Manuscript received June 24, 2015; revised February 22, 2016 and December 9, 2015; accepted April 14, 2016. Date of publication May 5, 2016; date of current version August 9, 2016. This work was supported in part by the National Natural Science Foundation of China under Grant 61375102, Grant 61333016, Grant 61421004, and Grant 61573226, and in part by the Beijing Natural Science Foundation under Grant 3141002 and Grant 4161002. *(Corresponding author: Junzhi Yu.)*

The authors are with the State Key Laboratory of Management and Control for Complex Systems, Institute of Automation, Chinese Academy of Sciences, Beijing 100190, China (e-mail: junzhi.yu@ia.ac.cn; yuanjun2012@ia.ac.cn; zhengxing.wu@ia.ac.cn; min.tan@ia.ac.cn).

Color versions of one or more of the figures in this paper are available online at http://ieeexplore.ieee.org.

Digital Object Identifier 10.1109/TIE.2016.2564338

ships [22], [23] and underwater vehicles [24], [25]. However, little research has been devoted to hydrodynamic parameters identification of swimming robots up to now.

This paper focuses on a data-driven dynamic modeling method for multijoint robotic fish with irregular geometric profiles and numerous heterogeneous hydrodynamic parameters. The novelty and contribution of this paper lies in two aspects. First, a dynamic model with an explicit form is derived, in which all terms involved in the dynamic analysis are converted to the coordinate system attached to the head. As a result, the form of the model is with better numerical stability for parameter search and dynamic simulation. During the dynamic modeling, a simple and intuitive hydrodynamic model, i.e., the Morison equation in coordination with the strip method, is adopted, which is proved to be effective via experiments. Second, the parameter identification technique is integrated into the modeling approach, which reshapes it with data-driven feature and thereby makes it be competent to model swimming robots with complex and irregular geometric profiles and numerous heterogeneous hydrodynamic parameters. The parameters are identified from experimental motion data directly, which solves the problem that they are difficult to settle. The obtained dynamic model is validated by motion data captured under extensive motion modes like forward swimming, varying velocity, and turning.

The remainder of the paper is organized as follows. Section II presents the structure and configuration of the multijoint robotic fish. Thereafter, the dynamic model is derived in Section III. Section IV elaborates on the identification approach of hydrodynamic parameters. In Section V, we evaluate the obtained dynamic model and parameters by comparing numerical simulations with aquatic experiments. Finally, conclusions are summarized in Section VI.

II. Overview of the Developed Robotic Fish

The dynamic modeling is implemented toward a multijoint swimming robotic fish developed in our laboratory [26]. The robotic fish is designed as a streamlined shape inspired by an *Esox lucius*, whose mechanical structure and appearance are illustrated in Fig. 1. Mechanically, the robot is composed of a rigid head and a self-propulsive body. Both the head and the body are covered by a compliant waterproof skin made of emulsion, in order to protect the internal mechanism from water. The two-degree-of-freedom pectoral mechanism and the novel neck joint can generate excellent 3-D maneuverability. But we always keep them still, since only planar motion is concerned in this paper.

The internal mechanism in the undulating body is essentially a multilink hinge structure, which is composed of four aluminum skeletons connected in series along the body. The posterior body is ended with a rigid caudal fin fixed to the last link via a slim peduncle. Such a configuration generates totally four rotatable joints within the flexible body, which are actuated by servomotors with strong torque and high speed. Motion of the robotic fish is controlled by a microcontroller embedded in the head. Red and yellow color markers made of waterproof material are attached to the head skin out of the rigid shell, as shown in Fig. 1(b). It is through tracking the color markers that we locate the robotic fish and acquire its motion data.

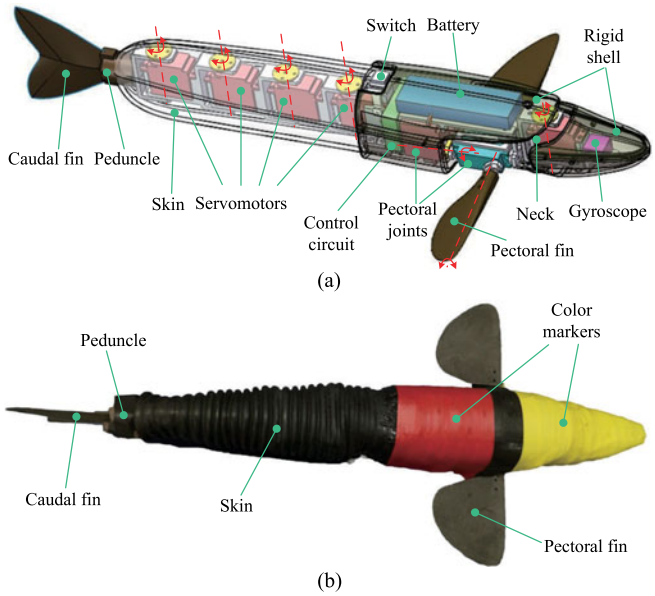

Fig. 1. Illustration of the developed multijoint robotic fish. (a) Mechanical structure. (b) Prototype with color markers.

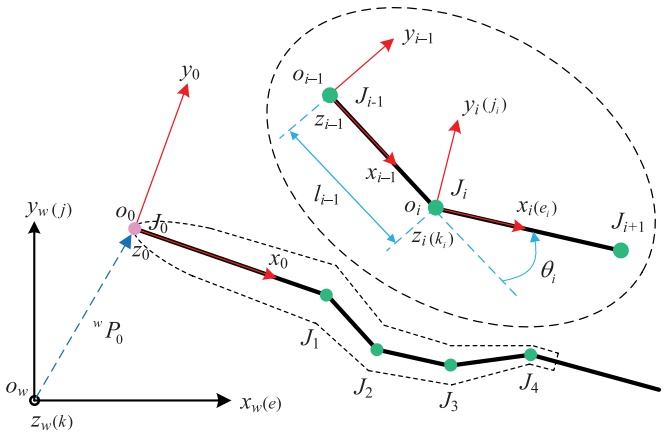

Fig. 2. Schematic illustration of coordinate systems and notation.

III. Dynamic Modeling

A. Coordinate Frames and Notation

Coordinate frames and notation involved in the following analysis of kinematics and dynamics are illustrated in Fig. 2. A world coordinate frame, denoted by $C_w = (o_w, x_w, y_w, z_w)$, is attached to the motion environment with the plane $o_w x_w y_w$ fixed on the water surface. The axis z_w is normal to the plane $o_w x_w y_w$. The unit vectors along corresponding axes are denoted by $\boldsymbol{e}$, $\boldsymbol{j}$, and $\boldsymbol{k}$. The robotic fish is simplified as a combination of five actuated links connected in series, each of which represents a body segment. A mobile frame $C_i = (o_i, x_i, y_i, z_i)$ is attached

to each body segment B_i, i indicates the ith body segment and $i \in [0, n]$, where n is the number of joints ($n = 4$). Especially, B_0 denotes the head of the robotic fish and the origin o_0 locates on the head's apex. For other body-fixed frame C_i ($i \neq 0$), the origin o_i is overlapped with the center of joint J_i. The length of B_i is a constant denoted by l_i. The joint angle of J_i is notated by θ_i. Particularly, θ_0 represents the yaw angle of the head.

We will utilize the following notation convention throughout all the mathematical formulation. The temporal derivative operator $d./dt$ is simplified as a dot over the head of a variable. With regard to the cross product of two vectors $\boldsymbol{a}, \boldsymbol{b} \in \Re^3$, the skew-symmetric matrix is introduced: $\boldsymbol{a} \times \boldsymbol{b} = \hat{\boldsymbol{a}} \cdot \boldsymbol{b}$, where $\hat{\boldsymbol{a}}$ denotes the corresponding (3×3) skew-symmetric matrix of $\boldsymbol{a}$. Additionally, the left superscript of a physical tensor indicates the projection frame. For instance, ${}^{w}R_0$ and ${}^{w}P_0$ denote the orientation matrix and position vector of C_0 with respect to C_w. When a tensor related to a link is expressed in the frame attached to this link, we omit its left superscript. Regarding expression of forces, torque is contained in a (6×1) generalized force vector if no special description is given.

B. Kinematic Analysis

The kinematics of our robotic fish are consistent with those of the swimming robot in [12] since such two robots share similar structures. According to the structure of the robotic fish, the orientation matrix and position vector of frame C_i with respect to C_{i-1} are given as follows:

$$ {}^{i-1}R_i = \begin{pmatrix} \cos\theta_i & -\sin\theta_i & 0 \\ \sin\theta_i & \cos\theta_i & 0 \\ 0 & 0 & 1 \end{pmatrix}, \; {}^{i-1}P_i = \begin{pmatrix} l_{i-1} \\ 0 \\ 0 \end{pmatrix}. $$

Through forward kinematic derivation, the velocity relation between two adjacent bodies is formalized by the recursive equation as follows:

$$ V_i = \begin{pmatrix} U_i \\ \Omega_i \end{pmatrix} = {}^{i}T_{i-1} V_{i-1} + \dot{\theta}_i K_i \tag{1} $$

where V_i is a (6×1) vector which denotes the velocity of body segment B_i expressed in frame C_i, U_i is the (3×1) linear velocity of origin o_i, Ω_i is the (3×1) angular velocity of B_i, $K_i = [\mathbf{0}_{3\times1}{}^T, \boldsymbol{k}_i{}^T]^T$ is a (6×1) unit vector, and ${}^{i}T_{i-1}$ is a (6×6) transformation matrix as follows:

$$ {}^{i}T_{i-1} = \begin{pmatrix} {}^{i}R_{i-1} & -{}^{i}R_{i-1}\,{}^{i-1}\hat{P}_i \\ \mathbf{0}_{3\times3} & {}^{i}R_{i-1} \end{pmatrix} \tag{2} $$

yeswhere ${}^{i}R_{i-1} = {}^{i-1}R_i{}^T$.

The recursive relation of acceleration can be further derived by implementing a temporal derivative operation on (1)

$$ \dot{V}_i = {}^{i}T_{i-1}\dot{V}_{i-1} + \xi_i + \ddot{\theta}_i K_i \tag{3} $$

where ξ_i is the result of ${}^{i}\dot{T}_{i-1} V_{i-1}$ (see the Appendix for details)

$$ \xi_i = \begin{pmatrix} [{}^{i}R_{i-1} \cdot (U_{i-1} - {}^{i-1}P_i \times \Omega_{i-1})] \times \dot{\theta}_i \boldsymbol{k}_i \\ ({}^{i}R_{i-1} \cdot \Omega_{i-1}) \times \dot{\theta}_i \boldsymbol{k}_i \end{pmatrix}. \tag{4} $$

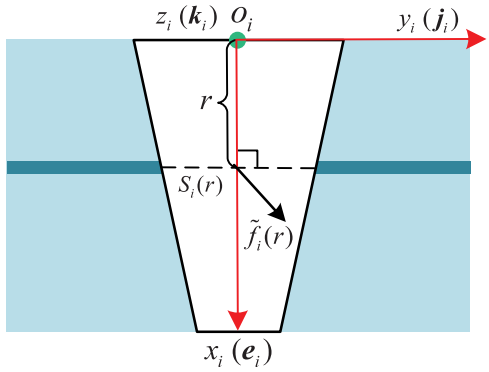

Fig. 3. Illustration of the 2-D hydrodynamic force exerted by a fluid slice.

Provided with V_0, $\dot{V}_0$, and rotation states of the joints, i.e., $\{(\theta_i, \dot{\theta}_i, \ddot{\theta}_i) | i \in [1, n]\}$, we can obtain the velocity and acceleration of each body segment by (1) and (3).

The conversion relations between V_0 and ${}^{w}V_0$ as well as $\dot{V}_0$ and ${}^{w}\dot{V}_0$ are as follows:

$$ {}^{w}V_0 = {}^{w}T_0 V_0 \tag{5} $$

$$ {}^{w}\dot{V}_0 = {}^{w}T_0 \dot{V}_0 + \begin{pmatrix} {}^{w}\Omega_0 \times {}^{w}U_0 \\ \mathbf{0}_{3\times1} \end{pmatrix} \tag{6} $$

where

$$ {}^{w}T_0 = \begin{pmatrix} {}^{w}R_0 & \mathbf{0}_{3\times3} \\ \mathbf{0}_{3\times3} & {}^{w}R_0 \end{pmatrix}. $$

C. Hydrodynamic Model

The robotic fish propels itself by external hydrodynamic forces, which is due to the interaction between the entire body and the surrounding liquid. To avoid complicated calculation of the hydrodynamics, some fundamental assumptions are made to the fluid-structure interaction. The fluid is assumed to be incompressible and irrotational. Owing to the slender geometric profile of the robotic fish, the slender-body theory [27] will be applied to the following analysis. That is, the surrounding fluid flow can be approximatively cut into continuous slices of planar flows transverse along the backbone of the body. According to the strip method [28], the hydrodynamic forces on the body can be further simplified as the superposition of the forces exerted on each cross section, as illustrated in Fig. 3. Definitely, as only planar motion is concerned in this paper, the rolling inertia and vertical cross-sectional inertia will not be involved in the hydrodynamic analysis.

The Morrison equation [28] is applied to model the hydrodynamic forces, which contain two components: the added mass force and the drag force. The former appears when the surrounding fluid is accelerated by the movement of the robotic fish. The latter comes from the friction viscosity and pressure difference on the body-fluid boundary.

The (6×1) added mass force exerted on the cross section $S_i(r)$ with respect to frame C_i can be formalized as follows:

$$ \tilde{\boldsymbol{f}}_{ad,i}(r) = -\tilde{M}_{ad,i}(r)\dot{V}_i - \tilde{\boldsymbol{\gamma}}_{ad,i}(r) \tag{7} $$

where r is the distance from o_i to $S_i(r)$, $\tilde{M}_{ad,i}(r)$ denotes the (6×6) added inertia matrix of the fluid slice around $S_i(r)$

$$\tilde{M}_{ad,i}(r)=\begin{pmatrix}\boldsymbol{m}_{a,i}(r) & -r\cdot\boldsymbol{m}_{a,i}(r)\hat{\boldsymbol{e}}_i\\ r\hat{\boldsymbol{e}}_i\cdot\boldsymbol{m}_{a,i}(r) & r^2\hat{\boldsymbol{e}}_i^T\boldsymbol{m}_{a,i}(r)\hat{\boldsymbol{e}}_i+I_{a,i}(r)\end{pmatrix}$$

$\tilde{\boldsymbol{\gamma}}_{ad,i}(r)$ indicates the (6×1) Coriolis–centrifugal force

$$\begin{aligned}\tilde{\boldsymbol{\gamma}}_{ad,i}(r)&=\begin{pmatrix}\hat{\Omega}_i & \mathbf{0}_{3\times3}\\ \mathbf{0}_{3\times3} & \hat{\Omega}_i\end{pmatrix}(\tilde{M}_{ad,i}(r)V_i)\\&=\begin{pmatrix}\hat{\Omega}_i\boldsymbol{m}_{a,i}(r) & -r\hat{\Omega}_i\boldsymbol{m}_{a,i}(r)\hat{\boldsymbol{e}}_i\\ r\hat{\Omega}_i\hat{\boldsymbol{e}}_i\boldsymbol{m}_{a,i}(r) & \hat{\Omega}_i(r^2\hat{\boldsymbol{e}}_i^T\boldsymbol{m}_{a,i}(r)\hat{\boldsymbol{e}}_i+I_{a,i}(r))\end{pmatrix}V_i\end{aligned}$$

$\boldsymbol{m}_{a,i}(r)$ is the (3×3) added mass matrix which depends on the dimensionless inertia coefficient $c_{m,i}$, the immersed height $h_i(r)$ of $S_i(r)$, and the fluid density ρ

$$\boldsymbol{m}_{a,i}(r)=\frac{1}{4}c_{m,i}\rho\pi h_i(r)^2(\boldsymbol{j}_i\cdot\boldsymbol{j}_i{}^T)\tag{8}$$

and $I_{a,i}(r)$ is the added angular inertia.

The drag force produced by the fluid slice is as follows:

$$\begin{aligned}{}^l\tilde{\boldsymbol{f}}_{dr,i}(r)=&-\frac{1}{2}\begin{pmatrix}I_{3\times3} & \mathbf{0}_{3\times3}\\ r\hat{\boldsymbol{e}}_i & I_{3\times3}\end{pmatrix}\cdot\\&\begin{pmatrix}c_{1,i}\,|v_{x,i}(r)|\,v_{x,i}(r)\boldsymbol{e}_i+c_{2,i}\,|v_{y,i}(r)|\,v_{y,i}(r)\boldsymbol{j}_i\\ \mathbf{0}_{3\times1}\end{pmatrix}\end{aligned}\tag{9}$$

where

$$\begin{cases}v_{x,i}(r)=(U_i+\Omega_i\times r\boldsymbol{e}_i)^T\cdot\boldsymbol{e}_i\\ v_{y,i}(r)=(U_i+\Omega_i\times r\boldsymbol{e}_i)^T\cdot\boldsymbol{j}_i\end{cases}$$

and

$$\begin{cases}c_{1,i}=c_{f,i}\rho p_i(r)\\ c_{2,i}=c_{d,i}\rho h_i(r)\end{cases}\tag{10}$$

where $c_{f,i}$ and $c_{d,i}$ are the dimensionless friction coefficient and drag coefficient, respectively, and $p_i(r)$ is the perimeter of the cross section $S_i(r)$.

The hydrodynamic force $\tilde{\boldsymbol{f}}_i(r)$ exerted on the cross section $S_i(r)$ can be obtained by summing the added mass force and the drag force

$$\tilde{\boldsymbol{f}}_i(r)=\tilde{\boldsymbol{f}}_{ad,i}(r)+\tilde{\boldsymbol{f}}_{dr,i}(r).\tag{11}$$

According to the strip method, the hydrodynamic force F_i exerted on the entire body segment B_i can be further derived by integrating $\tilde{\boldsymbol{f}}_i(r)$ along axis x_i

$$F_i=\int_0^{l_i}(\tilde{\boldsymbol{f}}_{ad,i}(r)+\tilde{\boldsymbol{f}}_{dr,i}(r))dr.\tag{12}$$

To facilitate the subsequent derivation, F_i is formalized concisely as

$$F_i=-M_{ad,i}\dot{V}_i-\boldsymbol{\gamma}_{ad,i}+\boldsymbol{f}_{dr,i}\tag{13}$$

where $M_{ad,i}$ is the added inertia matrix of body B_i

$$M_{ad,i}=\int_0^{l_i}\tilde{M}_{ad,i}(r)dr$$

$\boldsymbol{\gamma}_{ad,i}$ and $\boldsymbol{f}_{dr,i}$ are velocity-related terms

$$\boldsymbol{\gamma}_{ad,i}=\int_0^{l_i}\tilde{\boldsymbol{\gamma}}_{ad,i}(r)dr,\ \boldsymbol{f}_{dr,i}=\int_0^{l_i}\tilde{\boldsymbol{f}}_{dr,i}(r)dr.$$

D. Dynamic Model

The Newton–Euler formulation is employed to analyze the dynamics of the robotic fish. The dynamic equation of body segment B_i is as follows:

$${}^iG_{i-1,i}=M_i\dot{V}_i+\boldsymbol{\gamma}_i-F_i+{}^iT_{i+1}{}^{i+1}G_{i,i+1}\tag{14}$$

where M_i is the inertia matrix of B_i

$$M_i=\begin{pmatrix}m_iI_{3\times3} & -c_im_i\hat{\boldsymbol{e}}_i\\ c_im_i\hat{\boldsymbol{e}}_i & {c_i}^2m_i\hat{\boldsymbol{e}}_i^T\hat{\boldsymbol{e}}_i+I_i\end{pmatrix}\tag{15}$$

m_i is the mass, c_i denotes the distance between o_i and the mass center of B_i which is supposed to be on axis x_i, I_i is the angular inertia of B_i with respect to the mass center, and $\boldsymbol{\gamma}_i$ is the Coriolis-centrifugal force

$$\boldsymbol{\gamma}_i=\begin{pmatrix}m_i\hat{\Omega}_i & -c_im_i\hat{\Omega}_i\hat{\boldsymbol{e}}_i\\ c_im_i\hat{\Omega}_i\hat{\boldsymbol{e}}_i & \hat{\Omega}_i({c_i}^2m_i\hat{\boldsymbol{e}}_i^T\hat{\boldsymbol{e}}_i+I_i)\end{pmatrix}V_i.$$

${}^iG_{i-1,i}$ represents the force exerted on B_i by B_{i-1} with respect to frame C_i. Regarding the last body segment B_n, it is evident that

$$\begin{aligned}{}^lG_{n-1,n}&=M_n\dot{V}_n+\boldsymbol{\gamma}_n-F_n\\&=(M_n+M_{ad,n})\dot{V}_n+\boldsymbol{\gamma}_n+\boldsymbol{\gamma}_{ad,n}-\boldsymbol{f}_{dr,n}\end{aligned}\tag{16}$$

since ${}^{n+1}G_{n,n+1}=\mathbf{0}_{6\times1}$.

Substituting (16) into the dynamic equation of B_{n-1}, we can obtain

$$\begin{aligned}{}^{n-1}G_{n-2,n-1}=&(M_{n-1}+M_{ad,n-1})\dot{V}_{n-1}+\boldsymbol{\gamma}_{n-1}\\&+\boldsymbol{\gamma}_{ad,n-1}-\boldsymbol{f}_{dr,n-1}+{}^{n-1}T_n[(M_n+M_{ad,n})\dot{V}_n\\&+\boldsymbol{\gamma}_n+\boldsymbol{\gamma}_{ad,n}-\boldsymbol{f}_{dr,n}].\end{aligned}$$

Noticing that

$$\dot{V}_n={}^nT_{n-1}\dot{V}_{n-1}+\xi_n+\ddot{\theta}_nK_n$$

we can move a step further

$$\begin{aligned}{}^{n-1}G_{n-2,n-1}=&[{}^{n-1}T_n(M_n+M_{ad,n}){}^nT_{n-1}+M_{n-1}\\&+M_{ad,n-1}]\dot{V}_{n-1}+\boldsymbol{\gamma}_{n-1}+\boldsymbol{\gamma}_{ad,n-1}\\&-\boldsymbol{f}_{dr,n-1}+{}^{n-1}T_n[(M_n+M_{ad,n})(\xi_n+\ddot{\theta}_nK_n)\\&+\boldsymbol{\gamma}_n+\boldsymbol{\gamma}_{ad,n}-\boldsymbol{f}_{dr,n}].\end{aligned}$$

Executing such reverse recursion until it is the robot's head B_0, we can acquire

$$\begin{aligned}{}^0G_{-1,0}=&\sum_{i=0}^{n}[{}^iT_0{}^T(M_i+M_{ad,i}){}^iT_0]\dot{V}_0\\&+\sum_{i=0}^{n}{}^iT_0{}^T(\boldsymbol{\gamma}_i+\boldsymbol{\gamma}_{ad,i}-\boldsymbol{f}_{dr,i})\end{aligned}$$

$$+\sum_{i=1}^{n} {}^{i}T_0{}^{T}(M_i + M_{ad,i})\sum_{j=1}^{i} {}^{i}T_j(\xi_j + \ddot{\theta}_j K_j) \quad (17)$$

where ${}^{i}T_0 = {}^{i}T_{i-1}{}^{i-1}T_{i-2}\cdots{}^{1}T_0$, and ${}^{i}T_i = I_{6\times 6}$.

Eventually, by virtue of ${}^{0}G_{-1,0} = \mathbf{0}_{6\times 1}$, we can derive the acceleration of the head from (17)

$$\dot{V}_0 = -\mathrm{M}^{-1}\Gamma \quad (18)$$

where M denotes the inertia matrix of the whole robotic fish with respect to frame C_0 defined by

$$\mathrm{M} = \sum_{i=0}^{n} {}^{i}T_0{}^{T}(M_i + M_{ad,i}){}^{i}T_0 \quad (19)$$

and

$$\Gamma = \sum_{i=1}^{n} {}^{i}T_0{}^{T}(\boldsymbol{\gamma}_i + \boldsymbol{\gamma}_{ad,i} - \boldsymbol{f}_{dr,i}) + \sum_{i=1}^{n} {}^{i}T_0{}^{T}(M_i + M_{ad,i})\sum_{j=1}^{i} {}^{i}T_j(\xi_j + \ddot{\theta}_j K_j).$$

The head velocity V_0 is regarded as the state of the robotic fish. The dynamic model formalized in (18) describes the mapping relation between the joint space and the motion state in the time domain. Namely, the model takes the joint states and the head's velocity as the input and the state variable, respectively. Provided with the rotation law of the joints, i.e., $\{(\theta_i, \dot{\theta}_i, \ddot{\theta}_i)|i \in [1, n]\}$, we can simulate or predict the motion state of the robotic fish by the acquired dynamic model.

IV. Identification of Hydrodynamic Parameters

As introduced in Section II, the swimming robot is designed with a complex streamlined shape and multilink structure, which thereby leads to numerous heterogeneous hydrodynamic parameters. However, no existing reference data for such an irregular shape can help to obtain the parameters, and tuning manually will cost great effort. Thus, acquisition of these parameters is an obstacle that lies on the road of dynamic modeling. Identifying them directly from motion data of the robotic fish is a practical and convenient way. To gather the motion data, a motion measurement system [29] has been constructed by mounting a color video camera above a water pool. Motion information is captured by image sequences when the robotic fish is swimming freely. A tracking scheme is developed to continuously track the color markers attached on the robotic fish and calculate its pose.

The extracted motion data are the output of the dynamic model, while the input is the rotation law of the joints. Definitely, the rotation of the joints complies with a Hopf oscillator-based central pattern generator (CPG) model [30] as follows:

$$\begin{cases} \dot{\zeta}_i = -\omega_i(\psi_i - b_i) + \zeta_i[A_i - {\zeta_i}^2 - (\psi_i - b_i)^2] \\ \qquad +h_1[\zeta_{i-1}\cos\varphi_i + (\psi_{i-1} - b_{i-1})\sin\varphi_i] \\ \dot{\psi}_i = \omega_i\zeta_i + (\psi_i - b_i)[A_i - {\zeta_i}^2 - (\psi_i - b_i)^2] \\ \qquad +h_2[\zeta_{i+1}\sin\varphi_i + (\psi_{i+1} - b_{i+1})\cos\varphi_i] \\ \theta_i = \beta_i\psi_i \end{cases} \quad (20)$$

where ζ_i and ψ_i are the oscillation states of the ith oscillator, ω_i and A_i correspond to the intrinsic oscillation frequency and amplitude, respectively, h_1 and h_2 are the coupling weights, φ_i is the phase difference between adjacent oscillators, b_i denotes the directional bias, β_i is the magnification coefficient, and certainly θ_i is the output angle of the ith joint.

The hydrodynamic parameters which need to be determined are the inertia coefficient $c_{m,i}$ in (8), the friction coefficient $c_{f,i}$ and the drag coefficient $c_{d,i}$ in (10). It should be remarked that, in order to simplify the hydrodynamic analysis, we have ignored the influence of the Reynolds number and regarded the coefficients as constant. Actually, the coefficients are of complex relation with the Reynolds number. However, with respect to the robotic fish, the Reynolds number of each body segment during steady swimming is within a rough range of 10^4–10^5, and the coefficients maintain nearly constant in this range [31]. Hence, the simplification on the Reynolds number is reasonable for steady swimming stages. Regarding the robotic fish prototype introduced in Section II, we assume that the hydrodynamic parameters are identical for B_1, B_2, and B_3, considering the identity of the geometrical shapes and the skin material. Thus, there are a total of nine parameters remained to be settled in the dynamic model.

Indeed, the built dynamic model is a gray-box model with unknown parameters. We adopt a gray-box identification method [10] for parameter identification. Essentially, the identification process is to solve an optimization problem as follows:

$$\arg\min_{\lambda} \sum_{t} \varepsilon(t)^T W \varepsilon(t)$$
$$\text{s.t. } \lambda_l \le \lambda \le \lambda_u \quad (21)$$

where $\varepsilon(t)$ is the deviation between the experimental velocity $V_{0,e}(t)$ and the simulated velocity $V_{0,s}(t)$ at time t

$$\varepsilon(t) = V_{0,e}(t) - V_{0,s}(t)$$

λ is the set of hydrodynamic parameters:

$$\lambda = \{(c_{m,i},\, c_{d,i},\, c_{f,i})|i \in [0, n]\}$$

λ_l and λ_u are the lower and upper bound of λ, respectively, and W is a diagonal weight matrix which puts weight on each component of the velocities. The problem in (21) is solved by a nonlinear least-squares method based on the trust region reflective algorithm.

V. Experiments and Analysis

Identification of the hydrodynamic parameters is performed on motion data measured from aquatic experiments. The identification results and the obtained dynamic model are validated by comparing experimental data with the simulation results under different swimming modes.

A. Experimental Setup

Basic information of the robotic fish is tabulated in Section II. The robotic fish is composed of five body segments and four joints. Some physical parameters of each segment involved in the dynamic model are listed in Table I. The mass m_i and length

TABLE I
CONFIGURATION PARAMETERS OF THE ROBOTIC FISH

Item	Unit	B_0	B_1	B_2	B_3	B_4
m_i	Kg	1.528	0.159	0.159	0.171	0.091
l_i	m	0.291	0.062	0.062	0.062	0.137
c_i	m	0.18	0.044	0.044	0.045	0.037
$I_{i,z}$	$\mathrm{Kg}\cdot\mathrm{m}^2\,(\times 10^{-4})$	290	1.8	1.8	2.0	1.6

Note: the notation $I_{i,z}$ is the angular inertia with respect to the mass center along $\boldsymbol{k}_i$, and $I_i = I_{i,z}\,\boldsymbol{k}_i\,\boldsymbol{k}_i^T$.

TABLE II
PARAMETERS OF THE HOPF OSCILLATOR-BASED CPG

A_1	A_2	A_3	A_4	h_1	h_2	β	φ
8.70	19.07	25.49	40.39	4.0	5.0	60.0	70.0°

Note: the magnification coefficient β_i is equal to β for all the joints.

TABLE III
RESULTS OF HYDRODYNAMIC PARAMETER IDENTIFICATION

Item	$c_{m,0}$	$c_{m,1-3}$	$c_{m,4}$	$c_{d,0}$	$c_{d,1-3}$	$c_{d,4}$	$c_{f,0}$	$c_{f,1-3}$	$c_{f,4}$
λ_l	0.01	0.01	0.01	0.1	0.1	0.1	0.001	0.001	0.001
λ_u	3	3	3	4	4	4	0.02	0.02	0.02
λ_0	0.5	0.5	0.5	2	2	2	0.01	0.01	0.01
$\lambda^\star$	0.01	0.07	0.06	4	1.5	2.5	0.02	0.02	0.02

Note: the notation λ_0 denotes the initial value of λ, and $\lambda^\star$ represents the identified parameters.

l_i can be measured directly, whilst the mass center position c_i and the angular inertia $I_{i,z}$ are obtained from the mechanical model in Solidworks. Considering the irregularity of the robotic fish's geometry, we make some approximations to its geometrical shape to simplify calculation.

In addition, Table II lists a part of parameters of the Hopf oscillator-based CPG model in (20). These parameters are tuned in advance to achieve fish-like swimming within certain physical limitation of the mechanism. Definitely, they always keep constant throughout all the experiments. The remaining parameters need to be adjusted to change motion state or swimming mode of the robotic fish. Concretely, the intrinsic oscillation frequency ω_i controls the rotational frequency of each joints, which can further adjust the swimming speed. For all the joints, ω_i has the same value denoted by ω. The directional bias b_i is utilized to change the motion direction and turning radius.

B. Results of Hydrodynamic Parameter Identification

The identification of the hydrodynamic parameters is implemented on a piece of motion data, which is gathered when the robotic fish is swimming in accordance with specified motion mode. The weight matrix in (21) is set as $W = \mathrm{diag}(10^4,\ 10^4, 0, 0, 0, (180/\pi)^2)$, which changes the unit of the translational velocities from (m/s) to (cm/s) and changes that of the angular velocities from (rad/s) to (°/s). The lower bounds, upper bounds, and initial values of the hydrodynamic parameters λ are listed in Table III. The initial values are set according to the empirical values of structures with similar geometrical shapes [32]. Considering the nonlinearity of the optimization problem in (21), we restrict the range of the parameters to prevent the solution from drifting away. The bounds are determined by appropriately extending the ranges of empirical values. The implementation of identification is by virtue of the nonlinear gray-box identification tool in the system identification toolbox of MATLAB. Consequently, we obtain the identified hydrodynamic parameters $\lambda^\star$ listed in Table III. A part of parameters arrive the bounds, which is possibly due to the approximations made in the hydrodynamic and dynamic modeling. Additionally, the undulating tail is not completely rigid owing to the compliant skin, whose shape changes during swimming.

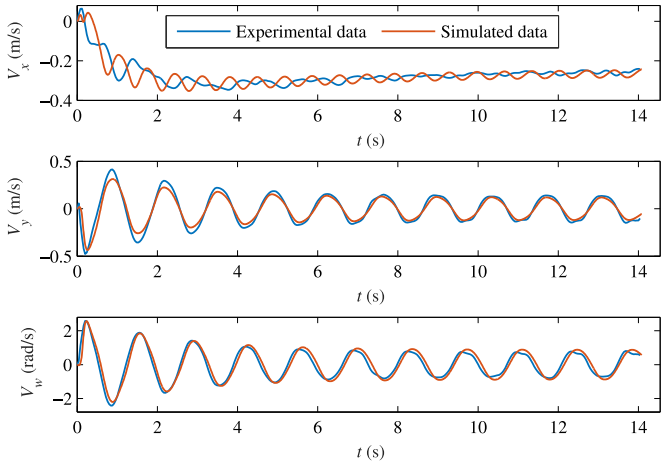

Fig. 4. Simulated and experimental velocities when the robotic fish is forward swimming ($\omega = 18$).

Substituting the identified hydrodynamic parameters into (18), we acquire a complete dynamic model. To validate the built model and identified parameters, we compare the simulated velocities with those measured from experiments. The ordinary differential equation (ODE) in (18) is highly nonlinear and lacks an analytical solution. Therefore, a numerical method, i.e., the ode45 solver in MATLAB, is applied to solve the ODE in practice. Generally, V_0 is with an initial value of zero and evolves with time during swimming simulations. The comparisons are implemented under different swimming modes of the robotic fish, as shown in Figs. 4–6. Fig. 4 displays the evolution of velocities with time when the robotic fish is swimming forward. The notation V_x and V_y denote the components of V_0 along x_0 and y_0, respectively, and V_w indicates the yaw velocity. Fig. 5 shows the case that the robotic fish decelerates by decreasing ω, i.e., the intrinsic oscillation frequency of CPG. Apparently, the head's swing frequency as well as the forward speed drops. Fig. 6 demonstrates the situation that the robotic fish performs a steady-state turning through adding a directional bias $\boldsymbol{b} = [b_1\ b_2\ b_3\ b_4]^T$. Vertical offsets appear in the curves of V_y and V_w, whilst V_x decreases when it begins to turn.

Intuitively, the simulated motion data match well with the measured data in the steady swimming stages, even though the robotic fish changes its motion mode. However, it is ob-

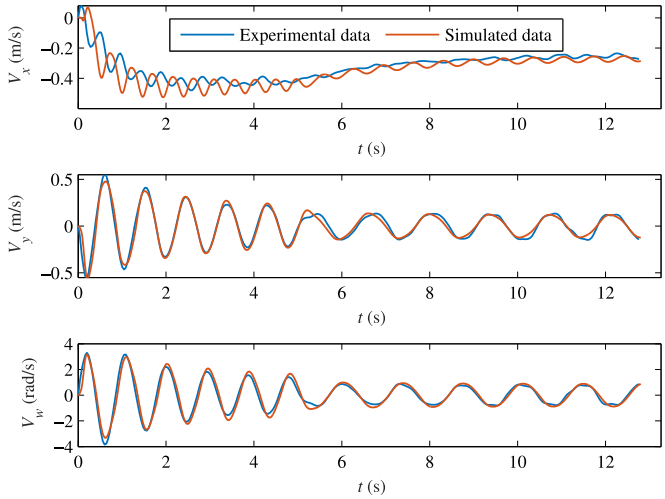

Fig. 5. Simulated and experimental velocities when the robotic fish decelerates (change $\omega = 26$ to $\omega = 18$) at 5.2 s during forward swimming.

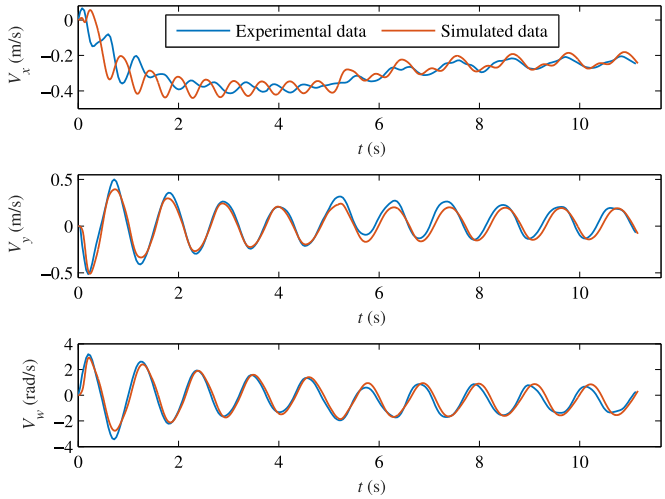

Fig. 6. Simulated and experimental velocities when the robotic fish performs a steady-state turning ($\omega = 22, \boldsymbol{b} = [0\,1\,1.5\,2]^T$) at 5.2 s.

served that some discrepancies appear in the startup stages. It is mainly attributed to two potential reasons. First, rolling movement with large amplitude appears during the quick startup of the robotic fish. But rolling has not been considered in the dynamic model, which leads to the discrepancies. Second, we have ignored the influence of Reynolds number and regarded the coefficients as constant. Those coefficients maintain nearly constant at the range of the Reynolds number corresponding to steady swimming stages, while they vary with the Reynolds number at startup stages since the Reynolds number is much lower. The identified parameters are close to the hydrodynamic coefficients in steady swimming stages. Hence, the simplification on the Reynolds number is another potential reason for the discrepancies in the startup stages.

To evaluate the accuracy of the built dynamic model quantitatively, we calculate the deviation between the simulated and experimental data, as listed in Table IV. The deviation refers

TABLE IV
DEVIATION BETWEEN THE SIMULATED AND EXPERIMENTAL MOTION DATA

Mode	ΔV_x (m/s)	ΔV_y (m/s)	ΔV_w (rad/s)	$\Delta \bar{V}_x$	$\Delta \bar{V}_y$	$\Delta \bar{V}_w$
v1	0.040	0.042	0.253	0.097	0.047	0.051
v3	0.051	0.044	0.349	0.105	0.043	0.056
v5	0.073	0.058	0.508	0.123	0.058	0.079
v7	0.095	0.073	0.619	0.142	0.068	0.084
v1-v5	0.053	0.035	0.298	0.117	0.045	0.059
v5-v1	0.062	0.038	0.276	0.111	0.034	0.039
v1-t1	0.041	0.036	0.245	0.109	0.045	0.048
v1-t2	0.041	0.046	0.304	0.115	0.059	0.061
v3-t1	0.047	0.041	0.198	0.100	0.046	0.034
v3-t2	0.057	0.054	0.335	0.119	0.053	0.051

Note: the notation "vx" corresponds to different ω, i.e., $\omega = 16 + 2x$, "t1" and "t2" correspond to $\boldsymbol{b} = [0\ 0.5\ 1\ 1.5]^T$ and $\boldsymbol{b} = [0\ 1\ 1.5\ 2]^T$ respectively. Mode "v1-v5" means that ω varies from 18 to 26 during motion. Mode "vx-tx" refers to the case that the robotic fish begins turning after a period of forward swimming.

to the root-mean-square error (RMSE) and normalized RMSE [10] defined below (take V_x, for instance)

$$\begin{cases} \Delta V_x = \sqrt{\frac{1}{N}\sum_t \left(V_{x,e}(t) - V_{x,s}(t)\right)^2} \\ \Delta \bar{V}_x = \Delta V_x / [\max(V_{x,e}) - \min(V_{x,e})] \end{cases}$$

where ΔV_x and $\Delta \bar{V}_x$ denote the RMSE and normalized RMSE of V_x, respectively, $V_{x,e}(t)$ and $V_{x,s}(t)$ are the experimental and simulated V_x at time t, and N is the number of samples.

It is shown from Table IV that the normalized RMSE on V_y is relatively lower than others. The dynamic model also shows good relative accuracy on V_w. Nevertheless, the normalized RMSE on V_x is a little higher, which is attributed to the deviation in the start-up stages that can be observed in Figs. 4–6. Additionally, the first four groups of data reveals that the deviation on almost all the three velocity components increases, while ω raises during forward swimming. One main reason is the roll movement of the robotic fish, which is not in consideration of our dynamic model. It is observed from experiments that the roll amplitude increases with ω. Turning motion also leads to roll movement. The higher the directional bias $\boldsymbol{b}$ is, the larger the roll amplitude arises. Thereby, the phenomenon that the deviation increases with $\boldsymbol{b}$ can be observed from the last four groups of turning-related data in Table IV.

C. Discussion

We have employed the Morrison equation to analyze the fluid forces exerted on the robotic fish. Compared with the adapted LAEBT model in [12], our analysis on hydrodynamics is simpler and more intuitive. Even though fewer fluid factors are considered in our hydrodynamic model, the experimental results have demonstrated its effectiveness to a certain extent. In addition, we have observed that the identified coefficients of the added mass are lower than normal empirical values. On the one hand, we have attributed such a phenomenon to the approximations which have been made in analysis. On the other hand, we conjecture that it may be more suitable to model the hydrodynamics by the quadratic terms of velocities than by the first-order dif-

ferential terms, in perspective of explaining the experimental motion data.

In the procedure of deriving the dynamic model, all terms involved in the dynamic analysis are converted to the coordinate frame attached to the head. Thereby, the dynamic model in (18) is with an explicit formulation. In comparison with the forward-backward recursion style in [12], the form in (18) has a merit of numerical stability, which is observed from experiments of parameter search and dynamic simulation. It is due to that an inversion operation of $(M_0 + M_{ad,0})$ need to be conducted to calculate $\dot{V}_0$ in the recursion algorithm, which leads to the numerical instability since the angular inertia term in $(M_0 + M_{ad,0})$ is of a very low value although we have tried robust methods to solve the dynamic equation of B_0. The form in (18) avoids this problem since M is the inertia matrix of the entire robotic fish as in (19) and thereby the angular inertia term is with a higher value.

The parameter identification technique reshapes the dynamic modeling method with data-driven feature, which can overcome the difficult in acquisition of the hydrodynamic parameters. By contrast, estimating by existing reference data for regular shapes [12] is not appropriate to robots with irregular geometric profiles, as like our swimming robot which is of a complex streamlined shape. Besides, each body segment of our robot is with different shapes and thereby different hydrodynamic parameters. Even though simplification and approximation on shapes are conducted, there still remain nine different parameters to be acquired. Tuning so many parameters manually to fit experimental data is tedious. The data-driven feature of our modeling approach makes the acquirement of numerous hydrodynamic parameters specific to irregular and complex geometric profiles feasible and convenient. Moreover, online parameter identification may be helpful to tackle the problem that hydrodynamic parameters vary in different swimming stages, and thereby achieve better modeling accuracy, which remains to be studied further in the future.

VI. Conclusion and Future Work

In this paper, we have presented a data-driven dynamic modeling method for multijoint robotic fish with irregular geometric profiles. This method consists of two parts: dynamic modeling and hydrodynamic parameter identification. For the dynamic modeling, we employ the Morrison equation and the strip method to analyze fluid forces. A dynamic model with an explicit form is derived, in which all terms involved in the dynamic analysis are converted to the coordinate system attached to the head. The form is with better numerical stability for parameter search and dynamic simulation. Nevertheless, the complex profiles and multilink structure lead to numerous heterogeneous hydrodynamic parameters which are difficult to settle. So we integrate the parameter identification technique into dynamic modeling. This data-driven feature makes it convenient and feasible to model swimming robots with complex geometric profiles. Experimental data are collected to identify the hydrodynamic parameters directly. To validate the built dynamic model and identified parameters, we compare the experimental data with the simulation results under extensive swimming modes. The comparisons have demonstrated the effectiveness of the dynamic model.

In the future, we will further validate the built dynamic model in more swimming modes including backward swimming and fast turning maneuvers. Meanwhile, we will study approaches for online parameter identification and optimization [33] to track the variation of parameters in different swimming stages. Furthermore, we plan to develop approaches for capturing 3-D motion data of the robotic fish so as to establish an accurate 3-D dynamic model.

Appendix

In this Appendix, we show the detailed procedure of deriving ξ_i in (4). Essentially, ξ_i is the result of ${}^i\dot{T}_{i-1}V_{i-1}$, which appears when deriving (3) from (1) via derivative operation

$$\begin{aligned}\xi_i &= {}^i\dot{T}_{i-1}V_{i-1} \\ &= \begin{pmatrix} -\dot{\theta}_i\hat{\boldsymbol{k}}_i{}^iR_{i-1} & \dot{\theta}_i\hat{\boldsymbol{k}}_i{}^iR_{i-1}{}^{i-1}\hat{P}_i - {}^iR_{i-1}{}^{i-1}\hat{\dot{P}}_i \\ \mathbf{0}_{3\times3} & -\dot{\theta}_i\hat{\boldsymbol{k}}_i{}^iR_{i-1} \end{pmatrix} V_{i-1}\end{aligned}$$

where we have utilized the equation ${}^i\dot{R}_{i-1} = (-\dot{\theta}_i\hat{\boldsymbol{k}}_i){}^iR_{i-1}$. Noting that ${}^{i-1}\dot{P}_i = \mathbf{0}_{3\times1}$, we can further obtain

$$\begin{aligned}\xi_i &= \begin{pmatrix} -\dot{\theta}_i\hat{\boldsymbol{k}}_i{}^iR_{i-1}U_{i-1} + \dot{\theta}_i\hat{\boldsymbol{k}}_i{}^iR_{i-1}{}^{i-1}\hat{P}_i\Omega_{i-1} \\ -\dot{\theta}_i\hat{\boldsymbol{k}}_i{}^iR_{i-1}\Omega_{i-1} \end{pmatrix} \\ &= \begin{pmatrix} -\dot{\theta}_i\boldsymbol{k}_i \times ({}^iR_{i-1}U_{i-1} - {}^iR_{i-1}({}^{i-1}P_i \times \Omega_{i-1})) \\ -\dot{\theta}_i\boldsymbol{k}_i \times ({}^iR_{i-1}\Omega_{i-1}) \end{pmatrix} \\ &= \begin{pmatrix} [{}^iR_{i-1}(U_{i-1} - {}^{i-1}P_i \times \Omega_{i-1})] \times \dot{\theta}_i\boldsymbol{k}_i \\ ({}^iR_{i-1}\Omega_{i-1}) \times \dot{\theta}_i\boldsymbol{k}_i \end{pmatrix}.\end{aligned}$$

Acknowledgment

The authors would like to thank the anonymous reviewers and the Associate Editor for their valuable comments and suggestions on revising this paper.

References

[1] J. Yu, M. Tan, S. Wang, and E. Chen, "Development of a biomimetic robotic fish and its control algorithm," *IEEE Trans. Syst. Man, Cybern. B, Cybern.*, vol. 34, no. 4, pp. 1798–1810, Aug. 2004.

[2] X. Niu, J. Xu, Q. Ren, and Q. Wang, "Locomotion learning for an anguilliform robotic fish using central pattern generator approach," *IEEE Trans. Ind. Electron.*, vol. 61, no. 9, pp. 4780–4787, Sep. 2014.

[3] J. Yu, C. Wang, and G. Xie, "Coordination of multiple robotic fish with applications to underwater robot competition," *IEEE Trans. Ind. Electron.*, vol. 63, no. 2, pp. 1280–1288, Feb. 2016.

[4] J. Yu, F. Sun, D. Xu, and M. Tan, "Embedded vision guided 3-D tracking control for robotic fish," *IEEE Trans. Ind. Electron.*, vol. 63, no. 1, pp. 355–363, Jan. 2016.

[5] W. Wang and G. Xie, "Online high-precision probabilistic localization of robotic fish using visual and inertial cues," *IEEE Trans. Ind. Electron.*, vol. 62, no. 2, pp. 1113–1124, Feb. 2015.

[6] L. Wen, T. Wang, G. Wu, and J. Liang, "Novel method for the modeling and control investigation of efficient swimming for robotic fish," *IEEE Trans. Ind. Electron.*, vol. 59, no. 8, pp. 3176–3188, Aug. 2012.

[7] J. Yu, M. Wang, Z. Su, M. Tan, and Jianwei Zhang, "Dynamic modeling of a CPG-governed multijoint robotic fish," *Adv. Robot.*, vol. 27, no. 4, pp. 275–285, 2013.

[8] F. Boyer, M. Porez, A. Leroyer, and M. Visonneau, "Fast dynamics of an eel-like robot—Comparisons with Navier-Stokes simulations," *IEEE Trans. Robot.*, vol. 24, no. 6, pp. 1274–1288, Dec. 2008.
[9] J. Wang and X. Tan, "A dynamic model for tail-actuated robotic fish with drag coefficient adaptation," *Mechatronics*, vol. 23, no. 6, pp. 659–668, 2013.
[10] V. Kopman, J. Laut, F. Acquaviva, A. Rizzo, and M. Porfiri, "Dynamic modeling of a robotic fish propelled by a compliant tail," *IEEE J. Ocean. Eng.*, vol. 40, no. 1, pp. 209–221, Jan. 2014.
[11] W. Khalil, G. Gallot, and F. Boyer, "Dynamic modeling and simulation of a 3-D serial eel-like robot," *IEEE Trans. Syst., Man, Cybern. C, Appl. Rev.*, vol. 37, no. 6, pp. 1259–1268, Nov. 2007.
[12] M. Porez, F. Boyer, and A. Ijspeert, "Improved Lighthill fish swimming model for bio-inspired robots: Modeling, computational aspects and experimental comparisons," *Int. J. Robot. Res.*, vol. 33, no. 10, pp. 1322–1341, 2014.
[13] J. E. Colgate and K. M. Lynch, "Mechanics and control of swimming: A review," *IEEE J. Ocean. Eng.*, vol. 29, no. 3, pp. 660–673, Jul. 2004.
[14] G. Taylor, "Analysis of the swimming of long and narrow animals," *Proc. R. Soc. Lond. A*, vol. 214, pp. 158–183, 1952.
[15] T. Y. Wu, "Swimming of a waving plate," *J. Fluid Mech.*, vol. 10, no. 3, pp. 321–344, 1961.
[16] M. J. Lighthill, "Note on the swimming of slender fish," *J. Fluid Mech.*, vol. 9, no. 2, pp. 305–317, 1960.
[17] M. J. Lighthill, "Aquatic animal propulsion of high hydro-mechanical efficiency," *J. Fluid Mech.*, vol. 44, no. 2, pp. 265–301, 1970.
[18] M. J. Lighthill, "Large-amplitude elongated body theory of fish locomotion," *Proc. R. Soc. Lond. B*, vol. 179, no. 1055, pp. 125–138, 1971.
[19] Z. Chen, S. Shatara, and X. Tan, "Modeling of biomimetic robotic fish propelled by an ionic polymer–metal composite caudal fin," *IEEE/ASME Trans. Mechatronics*, vol. 15, no. 3, pp. 448–459, Jun. 2010.
[20] M. Aureli, V. Kopman, and M. Porfiri, "Free-locomotion of underwater vehicles actuated by ionic polymer metal composites," *IEEE/ASME Trans. Mechatronics*, vol. 15, no. 4, pp. 603–614, Aug. 2010.
[21] V. Kopman and M. Porfiri, "Design, modeling, and characterization of a miniature robotic fish for research and education in biomimetics and bioinspiration," *IEEE/ASME Trans. Mechatronics*, vol. 18, no. 2, pp. 471–483, Apr. 2013.
[22] H. K. Yoon and K. P. Rhee, "Identification of hydrodynamic coefficients in ship maneuvering equations of motion by estimation-before-modeling technique," *Ocean Eng.*, vol. 30, no. 18, pp. 2379–2404, 2003.
[23] M. H. Casado and R. Ferreiro, "Identification of the nonlinear ship model parameters based on the turning test trial and the backstepping procedure," *Ocean Eng.*, vol. 32, no. 11, pp. 1350–1369, 2005.
[24] J. Kim, K. Kim, H. S. Choi, W. Seong, and K.-Y. Lee, "Estimation of hydrodynamic coefficients for an AUV using nonlinear observers," *IEEE J. Ocean. Eng.*, vol. 27, no. 4, pp. 830–840, Oct. 2002.
[25] S. C. Martin and L. L. Whitcomb, "Experimental identification of six-degree-of-freedom coupled dynamic plant models for underwater robot vehicles," *IEEE J. Ocean. Eng.*, vol. 39, no. 4, pp. 662–671, Oct. 2014.
[26] Z. Wu, J. Yu, Z. Su, M. Tan, and Z. Li, "Towards an Esox lucius inspired multimodal robotic fish," *Sci. China Inf. Sci.*, vol. 58, no. 5, pp. 1–13, 2015.
[27] M. Adams, "Slender-body theory–Review and extension," *J. Aeron. Sci.*, vol. 20, no. 2, pp. 85–98, 2012.
[28] F. Hawary, *The Ocean Engineering Handbook*. Boca Raton, FL, USA: CRC Press, 2000.
[29] J. Yuan, J. Yu, Z. Wu, and M. Tan, "Precise planar motion measurement of a swimming multi-joint robotic fish," *Sci. China Inf. Sci.*, doi: 10.1007/s11432-015-5497-1, 2015, to be published.
[30] Z. Wu, J. Yu, M. Tan, and J. Zhang, "Kinematic comparison of forward and backward swimming and maneuvering in a self-propelled sub-carangiform robotic fish," *J. Bionic Eng.*, vol. 11, no. 2, pp. 199–212, 2014.
[31] S. F. Hoerner, *Fluid-Dynamic Drag: Practical Information on Aerodynamic Drag and Hydrodynamic Resistance*. Midland Park, NJ, USA: Hoerner Fluid Dynamics, 1965.
[32] T. Sarpkaya and M. Isaacson, *Mechanics of Wave Forces On Offshore Structures*. New York, NY, USA: Van Nostrand, 1981.
[33] J. Fu, J. Faust, B. Chachuat, and A. Mitsos, "Local optimization of dynamic programs with guaranteed satisfaction of path constraints," *Automatica*, vol. 62, pp. 184–192, 2015.

Junzhi Yu (SM'14) received the B.E. degree in safety engineering and the M.E. degree in precision instruments and mechanology from the North University of China, Taiyuan, China, in 1998 and 2001, respectively, and the Ph.D. degree in control theory and control engineering from the Institute of Automation, Chinese Academy of Sciences (IACAS), Beijing, China, in 2003.

He is currently a Professor with the State Key Laboratory of Management and Control for Complex Systems, IACAS. His research interests include biomimetic robots, intelligent control, and intelligent mechatonic systems.

Dr. Yu serves as an Associate Editor of the IEEE TRANSACTIONS ON ROBOTICS and *Journal of Mechanical Science and Technology*, and as a Technical Editor of the IEEE/ASME TRANSACTIONS ON MECHATRONICS.

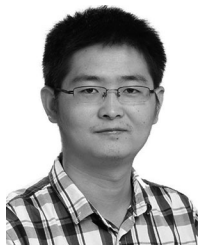

Jun Yuan received the B.E. degree in automation from Wuhan University, Wuhan, China, in 2012. He is currently working toward the Ph.D. degree in control theory and control engineering at the Institute of Automation, Chinese Academy of Sciences, Beijing, China.

His research interests include underwater robotics and intelligent control systems.

Zhengxing Wu received the B.E. degree from the School of Control Science and Engineering, Shandong University, Jinan, China, in 2008, and the Ph.D. degree in control theory and control engineering from the Institute of Automation, Chinese Academy of Sciences (IACAS), Beijing, China, in 2015.

He is currently an Assistant Professor with the State Key Laboratory of Intelligent Control and Management of Complex Systems, IACAS. His research interests include fast maneuvers of bioinspired robotic fish and gliding motions of robotic dolphins.

Min Tan received the B.Sc. degree from Tsinghua University, Beijing, China, in 1986, and the Ph.D. degree from the Institute of Automation, Chinese Academy of Sciences (IACAS), Beijing, in 1990, both in control science and engineering.

He is currently a Professor with the State Key Laboratory of Management and Control for Complex Systems, IACAS. He has published more than 200 papers in journals, books, and conference proceedings. His research interests include robotics and intelligent control systems.